Available online at www.sciencedirect.com
SCIENCE DIRECT®
International Journal of Heat and Mass Transfer 47 (2004) 4113–4123
International Journal of HEAT and MASS TRANSFER
www.elsevier.com/locate/ijhmt

Large eddy simulation of turbulent forced gas flows in vertical pipes with high heat transfer rates

Xiaofeng Xu [a], Joon Sang Lee [a], Richard H. Pletcher [b,*], A. Mohsen Shehata [c], Donald M. McEligot [d,e]

[a] Department of Mechanical Engineering, 2025 Black Engineering Building, Iowa State University, Ames, IA 50011, USA
[b] Department of Mechanical Engineering, 3024 Black Engineering Building, Iowa State University, Ames, IA 50011, USA
[c] Xerox Corporation, 800 Philips Road, 111-20N, Webster, NY 14580, USA
[d] Idaho National Engineering and Environmental Laboratory, Idaho Falls, ID 83415-3885, USA
[e] University of Arizona, Tucson, AZ 85721, USA

Received 22 December 2003; received in revised form 7 May 2004

Abstract

Large eddy simulation (LES) of vertical turbulent pipe flows with significant property variations has been performed to investigate the effects of high heat fluxes on the turbulent structures and transport. The Cartesian-based, compressible filtered Navier–Stokes equations were solved using a second-order accurate finite volume method. Low Mach number preconditioning was used to enable the compressible code to perform efficiently at low Mach numbers. A dynamic subgrid-scale stress model accounted for the subgrid-scale turbulence. In this study, the simulations were designed to simulate the experiments of Shehata and McEligot with three different near-constant heat fluxes. Step-periodic boundary conditions based on a quasi-developed assumption were used. The predicted integral parameters and mean velocity and temperature profiles agreed well with the experimental data. The fluid structures have been distorted due to high heat fluxes leading to significant property variations in the near wall region. The results showed that strong heating resulted in remarkable reductions of turbulent intensities, shear stresses, and turbulent heat flux. Apparent "laminarization" of the flow has been observed.

1. Introduction

Due to the advantages of safety, chemical inertness, and high thermal efficiency, gas coolants have been considered for nuclear reactors and heat exchangers for both fission and fusion applications. In some cases, these applications operate with turbulent flows at low Reynolds numbers with significant heat transfer rates resulting in large property variations. When the turbulent flow is strongly heated, it may revert to a laminar-like state where wall parameters approach the appropriate laminar values at local Reynolds numbers where turbulent flow is normally expected [1]. The transition from turbulent flow to laminar-like flow is sometimes referred to as laminarization [2,3].

Most experiments involving strong heating of gases have been conducted in tubes too small to permit measurements of detailed velocity and temperature profiles. In most cases, only integral measurements like heat transfer coefficient and/or friction factor were determined [1]. The first mean temperature profiles for dominantly forced convection of gases in a vertical pipe with significant property variations at low Mach numbers were measured by Perkins [4]. Shehata and McEligot [5] obtained the mean temperature and first mean velocity profiles for this situation to guide the development of predictive turbulence models. However, many

* Corresponding author. Tel.: +1-515-294-2656; fax: +1-515-294-3261.
E-mail address: pletcher@iastate.edu (R.H. Pletcher).

0017-9310/$ - see front matter © 2004 Published by Elsevier Ltd.
doi:10.1016/j.ijheatmasstransfer.2004.05.011

Nomenclature

A_c	pipe cross-sectional area, πR^2
B_j	buoyancy parameter, $Gr_q/(Re_b^{3.425}Pr^{0.8})$
C_d, C_I	dynamic subgrid-scale model coefficients
c_p	constant pressure specific heat
c_v	constant volume specific heat
D	pipe diameter
$\widehat{E}$	resolved total energy, $c_v\widetilde{T}+\frac{1}{2}\widetilde{u}_i\widetilde{u}_i$
G	mean mass flow flux, $\dot{m}/A_c$
Gr_q	Grashof number based on heat flux, $(gD^4q''_w)/(v_b^2k_bT_b)$
g	gravitational constant
h	heat transfer coefficient
K_v	local acceleration parameter, (v_b/u_b^2) (du_b/dx)
k	thermal conductivity
L_x	streamwise length of pipe
$\dot{m}$	mass flow rate
Nu	Nusselt number, hD/k
Pr	Prandtl number, $c_p\mu/k$
Pr_t	SGS turbulent Prandtl number
p	thermodynamic pressure
Q_j	SGS heat flux
$\hat{q}_j$	heat flux vector
q_{in}	nondimensional wall heat flux based on inlet conditions of experiments, $q''_w/(Gc_{p_{in}}T_{in})$
q''_w	wall heat flux
R	gas constant or radius of pipe
r	radial coordinate
Re	Reynolds number, $4\dot{m}/\pi D\mu$
$\widetilde{S}_{ij}$	strain rate tensor
T	thermodynamic temperature
T_b	bulk temperature, $\int \rho uT\,dA/(\rho_b u_b A_c)$
T_τ	friction temperature, $q''_w/(\rho_w c_p u_\tau)$
T_w	wall temperature
t	physical time
u, v, w	Cartesian velocity components in x, y, z directions
u, u_r, u_θ	velocity components in streamwise, radial, and circumferential directions
u_b	bulk streamwise velocity, $\int \rho u\,dA/(\rho_b A_c)$
u_τ	friction velocity, $\sqrt{\tau_w/\rho_w}$
x, y, z	Cartesian coordinates
y^+	distance from wall in wall coordinates, $(R-r)u_\tau/v_w$

Greek symbols

α, π, ε	subgrid-scale terms in energy equation
β	pressure gradient parameter
Δ	grid filter width
θ	temperature difference, $T_w - T$
μ	molecular dynamic viscosity
μ_t	subgrid-scale turbulent viscosity
v	kinetic viscosity, μ/ρ
ρ	thermodynamic density
ρ_b	bulk density, $\int \rho dA/A_c$
$\sigma_{i,j}$	shear stress tensor
τ	shear stress
τ_{ij}	subgrid-scale stress tensor

Subscripts

b	bulk property
con	conduction contribution
r	evaluated in radial direction
res	resolved contribution
rms	root-mean-square
sgs	subgrid-scale contribution
vis	viscous contribution
w	wall value
θ	evaluated in the circumferential direction of pipe

Superscripts and other symbols

+	wall coordinates
$''$	fluctuation with respect to Favre ensemble average quantity
–	resolved or large scale component of filtered quantity
$\sim$	resolved or large scale component of Favre filtered quantity
$\wedge$	quantity that is nonlinear function of Favre filtered quantities
$\hat{}$	test filtered quantity

Abbreviations

DNS	direct numerical simulation
LES	large eddy simulation
LU-SGS	lower–upper symmetric-Gauss-Seidel
MPI	message passing interface
SGS	subgrid-scale

proposed analytical and computational models provide poor predictions for convective heat transfer even when the properties can be idealized as constant [6], and it is very clear that the level of difficulty will be increased significantly if property variations and buoyancy forces are involved.

Direct numerical simulation (DNS) and large eddy simulation (LES) have provided means for obtaining detailed information about turbulent flows [7–11]. Satake et al. [12] performed DNS for a turbulent gas flow with variable properties to grasp and understand the laminarization phenomena caused by strong heating.

The goal of the present study is to investigate turbulent pipe flow with particular attention being paid to the effects of high heating rates on the mean and instantaneous structures. It is very expensive to perform LES for a developing pipe flow with high heat transfer. Consequently, the region of interest in this research is the "quasi-developed" region [13], where thermal entry effects are no longer important.

2. Governing equations

For gas flows in a tube with property variations (density, viscosity, and conductivity) in the axial and radial directions, the compressible Navier–Stokes equations are applicable even if a low speed case is treated. The governing equations for large eddy simulation are obtained by filtering the Cartesian-based compressible form of the equations for the conservation of mass, momentum, and energy. The equations are recast in terms of Favre averages (mass-weighted) and the body forces are included in the momentum and energy equations. The resulting set of equations governing the large eddy motion is

$$\frac{\partial\bar{\rho}}{\partial t}+\frac{\partial(\bar{\rho}\tilde{u}_j)}{\partial x_j}=0, \tag{1}$$

$$\frac{\partial(\bar{\rho}\tilde{u}_i)}{\partial t}+\frac{\partial(\bar{\rho}\tilde{u}_i\tilde{u}_j)}{\partial x_j}=-\frac{\partial\bar{p}}{\partial x_i}+\frac{\partial\bar{\sigma}_{ij}}{\partial x_j}-\bar{\rho}g\delta_{1i}-\frac{\partial\tau_{ij}}{\partial x_j}, \tag{2}$$

$$\frac{\partial(\bar{\rho}\widehat{E})}{\partial t}+\frac{\partial[(\bar{\rho}\widehat{E}+\bar{p})\tilde{u}_j]}{\partial x_j}=\frac{\partial(\tilde{u}_i\bar{\sigma}_{ij})}{\partial x_j}-\frac{\partial\bar{q}_j}{\partial x_j}-\bar{\rho}g\tilde{u}_i\delta_{1i}-\frac{\partial Q_j}{\partial x_j}-\alpha-\pi-\varepsilon, \tag{3}$$

and the equation of state is

$$\bar{p}=R\bar{\rho}\widetilde{T}. \tag{4}$$

The effects of the small-scale motions are present in the above equations through the subgrid-scale (SGS) stress tensor, τ_{ij}, in the momentum equation as

$$\tau_{ij}=\bar{\rho}(\widetilde{u_iu_j}-\tilde{u}_i\tilde{u}_j) \tag{5}$$

and the SGS terms that are the last four terms on the right-hand side of Eq. (3) (energy equation) as

$$Q_j=\bar{\rho}c_v(\widetilde{Tu_j}-\widetilde{T}\tilde{u}_j), \tag{6}$$

$$\alpha=\tilde{u}_i\frac{\partial\tau_{ij}}{\partial x_j}, \tag{7}$$

$$\pi=\overline{p\frac{\partial u_j}{\partial x_j}}-\bar{p}\frac{\partial\tilde{u}_j}{\partial x_j}, \tag{8}$$

$$\varepsilon=\overline{\sigma_{ij}\frac{\partial u_i}{\partial x_j}}-\hat{\sigma}_{ij}\frac{\partial\tilde{u}_j}{\partial x_j}, \tag{9}$$

where Q_j is the SGS heat flux vector. For the present work, it is appropriate to neglect α, π and ε since only low Mach number flows were considered [14].

The filtered dimensionless viscous stress and heat flux vectors are approximated by assuming that the correlations between the fluid properties and the derivatives of the velocity or temperature are weak [15]. The approximations are

$$\bar{\sigma}_{ij}\approx\hat{\sigma}_{ij}=2\bar{\mu}\left(\widetilde{S}_{ij}-\frac{1}{3}\widetilde{S}_{kk}\delta_{ij}\right) \tag{10}$$

and

$$\bar{q}_j\approx\hat{q}_j=-\frac{c_p\bar{\mu}}{P_r}\frac{\partial\widetilde{T}}{\partial x_j}, \tag{11}$$

where the strain rate tensor is

$$\widetilde{S}_{ij}=\frac{1}{2}\left(\frac{\partial\tilde{u}_i}{\partial x_j}+\frac{\partial\tilde{u}_j}{\partial x_i}\right). \tag{12}$$

To close the system of equations, the SGS stress tensor and heat flux vector in the Favre-filtered equations need be modeled. In this paper, the dynamic model proposed for compressible turbulence by Moin et al. [16] and recommended by Lilly [17] was implemented.

The anisotropic part of the SGS stress tensor based on the grid filter can be modeled as

$$\tau_{ij}-\frac{1}{3}\tau_{kk}\delta_{ij}=-2C_d\bar{\rho}\Delta^2|\widetilde{S}|\left(\widetilde{S}_{ij}-\frac{1}{3}\widetilde{S}_{kk}\delta_{ij}\right). \tag{13}$$

The isotropic part of the SGS stress tensor, τ_{kk}, was neglected here because it is negligible compared to the thermodynamic pressure [16]. Unlike the Smagorinsky model, the model coefficient, C_d, is computed dynamically by using spectral information contained in the resolved field through the use of two different scales, the grid scale and a larger "test filter" scale, yielding

$$C_d=\frac{\langle L_{ij}M_{ij}\rangle}{\langle M_{kl}M_{kl}\rangle}, \tag{14}$$

where

$$L_{ij}=\widehat{\bar{\rho}\tilde{u}_i\tilde{u}_j}-\frac{\widehat{\bar{\rho}\tilde{u}_i}\,\widehat{\bar{\rho}\tilde{u}_j}}{\hat{\bar{\rho}}}, \tag{15}$$

$$M_{ij}=-2\hat{\bar{\rho}}\widehat{\Delta}^2|\widehat{\widetilde{S}}|\left(\widehat{\widetilde{S}}_{ij}-\frac{1}{3}\widehat{\widetilde{S}}_{kk}\delta_{ij}\right)+2\Delta^2\bar{\rho}|\widetilde{S}|\left(\widetilde{S}_{ij}-\widehat{\frac{1}{3}\widetilde{S}_{kk}\delta_{ij}}\right) \tag{16}$$

and $\langle\ \rangle$ denotes a spatial averaging procedure along the homogeneous directions of the flow to make the SGS coefficients well conditioned. The test filter width, $\widehat{\Delta}$, is defined in the same way as the grid filter width, Δ, and is

equal to twice the grid filter width. The quantities with the symbol $\widetilde{}$ or $\widehat{}$ are the filtered variables obtained from the resolved field.

A procedure similar to the modeling of the SGS stress tensor is followed to represent the SGS heat flux vector, which can be modeled as

$$Q_j = -\frac{c_p \mu_t}{Pr_t}\frac{\partial \widetilde{T}}{\partial x_j} = -\frac{c_p C_d \bar{\rho}\Delta^2 |\widetilde{S}|}{Pr_t}\frac{\partial \widetilde{T}}{\partial x_j}, \tag{17}$$

where Pr_t is the turbulent Prantl number that is calculated dynamically as

$$Pr_t = -c_p C_d \frac{\langle F_j F_j \rangle}{\langle H_k F_k \rangle}, \tag{18}$$

where

$$H_j = c_v\left(\widehat{\bar{\rho}\tilde{u}_j\widetilde{T}} - \frac{\widehat{\overline{\rho u_j}}\,\widehat{\overline{\rho T}}}{\hat{\bar{\rho}}}\right), \tag{19}$$

$$F_j = \hat{\bar{\rho}}\widehat{\Delta}^2|\widehat{\widetilde{S}}|\frac{\partial \hat{\widetilde{T}}}{\partial x_j} - \Delta^2\left(\widehat{\bar{\rho}|\widetilde{S}|\frac{\partial \widetilde{T}}{\partial x_j}}\right). \tag{20}$$

3. Finite volume formulation

A coupled finite volume method was used to solve the filtered compressible Navier–Stokes equations based on Cartesian coordinates [18]. The code used non-Cartesian hexahedral and tetrahedral control volumes created based on cylindrical coordinates and solved for the primitive variables (p, u, v, w, T) which were stored at the cell centers. Time integration was performed using an implicit LU-SGS scheme in a dual time-stepping approach. Time-derivative preconditioning was used to enable the computation of low Mach number flows with property variations. The solver was second-order accurate in space and time. The multiblock code was parallelized using the message passing interface (MPI). This approach has been successfully tested on isothermal turbulent pipe flow [19], and the results have shown good agreement with DNS [20] and measurements [21].

4. Boundary conditions

The governing equations require specification of boundary conditions at the wall, inlet, and outlet due to the elliptic nature of the equations. Nonslip wall conditions are imposed at the wall. The fixed wall temperature distributions were specified according to experimental data. Since quasi-developed pipe flow is assumed in this study, step-periodic boundary conditions are used at the inlet and outlet as follows:

$$\begin{aligned} p_p(0,y,z) &= p_p(L_x,y,z)\\ \rho u(0,y,z) &= \rho u(L_x,y,z)\\ v(0,y,z) &= v(L_x,y,z)\\ w(0,y,z) &= w(L_x,y,z)\\ T(0,y,z) &= T(L_x,y,z) - \Delta T_x, \end{aligned} \tag{21}$$

where L_x is the length of pipe and p_p is the periodic component of the pressure, $p(x,y,z) = \beta x + p_p(x,y,z)$. With small property variations, the temperature difference, ΔT_x, can be approximated by the streamwise change in the bulk temperature as

$$\Delta T_x \approx \Delta T_b = \frac{4 q''_w L_x}{G c_p D}, \tag{22}$$

here D is the pipe diameter, q''_w is wall heat flux, and G is the mean mass flow flux. However, ΔT_x is a function of r when the property variations are significant. Referring to the experimental data, the profile of ΔT_x in the cross section of a pipe could be a function with different exponents at different locations. In this work, it was assumed as

$$\Delta T_x(r) = c_1 r^n + c_2. \tag{23}$$

It is difficult to determine the value of the exponent, n, required in order to approximate a desired state. Several trials were required to obtain a useful exponent and wall temperature distribution to match with the experimental data. By specifying wall streamwise temperature difference along the wall, ΔT_w, and bulk temperature rise, ΔT_b, for the pipe, the constants c_1 and c_2 were calculated as discussed by Xu [18], yielding

$$c_1 = \frac{\Delta T_b - \Delta T_w}{I_{\rho u r} - R^n}, \tag{24}$$

$$c_2 = \frac{I_{\rho u r}\Delta T_w - R^n \Delta T_b}{I_{\rho u r} - R^n}, \tag{25}$$

where

$$I_{\rho u r} = \frac{1}{\rho_b u_b A_c}\int \rho u r^n \mathrm{d}A|_{x=L_x}. \tag{26}$$

5. Results and discussion

Simulations were conducted for air flowing upwards in a vertical pipe as shown in Fig. 1. The experiments were conducted by Shehata and McEligot [5] at high heating rates causing significant property variations in the mixed convection in which the forced convection was dominant. Three characteristic cases, "turbulent", "subturbulent" and "laminarizing", were studied by Shehata and McEligot at different nondimensional heating rates of $q_{in} \approx 0.0018$, 0.0035 and 0.0045.

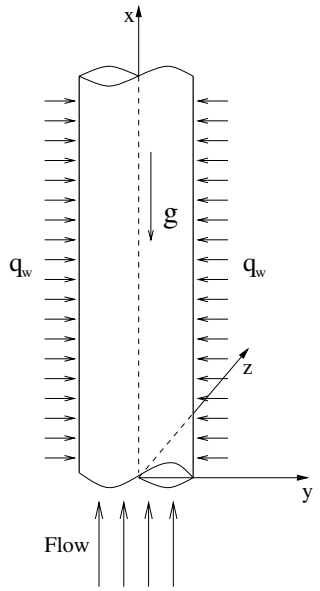

Fig. 1. The configuration of vertical pipe flow.

In this paper, six simulations with different constant heat fluxes were performed to approximately match with the experimental data of Shehata and McEligot [5]. The simulation conditions are tabulated in Table 1. In this table, x/D is the cross-section location of the experimental data used to compare with the corresponding simulation. The values of q_{in}, $T_w(0)$, dT_w/dx and dT_b/dx are all nondimensionalized with respect to the temperature at the start of heating in the experiment. The length of the computational domain was five times the pipe diameter. The grid resolution used in the simulations was $64\times40\times100$ in streamwise, radial, and circumferential directions, respectively. The grid spacing was uniform in the streamwise and circumferential directions, but was stretched towards the wall using the hyperbolic tangent algorithm. Turbulence statistics were collected using about $N_{stat} = 10,000$ time steps once the flow was deemed to be statistically stationary. The simulations were all run with nine processors on the Origin 3800 machine and required about 14–15 h of wall clock time per 5000 time steps.

Since flows with heat transfer are nonhomogeneous in the streamwise direction, all the averages in the following sections were made only in the circumferential direction and in time at each streamwise location. The bulk parameters of the current simulations and the corresponding experimental data [5] are shown in Tables 2 and 3, respectively. Although the buoyancy parameter for case 3 is slightly smaller than for experimental case 445, the comparison should still be of interest since forced convection effects are still dominant. Generally, the simulation parameters matched the experimental conditions well. The Nusselt number decreases when the heating rate increases because the viscous layer, which is responsible for the main thermal resistance, is thicker when the heating rate is higher. The Grashof number, local acceleration parameter and buoyancy parameter in the tables are defined as in the experiments, giving

$$Gr_q = \frac{gD^4 q''_w}{\nu_b^2 k_b T_b}, \tag{27}$$

$$K_v = \frac{\nu_b}{u_b^2}\frac{du_b}{dx}, \tag{28}$$

Table 1
Simulation parameters for LES

LES cases	x/D	n	q_{in}	$T_w(0)$	dT_w/dx	dT_b/dx
1	14.195	2	1.8×10^{-3}	1.47	3.973×10^{-3}	3.6×10^{-3}
2	19.87	2	3.5×10^{-3}	2.18	1.05×10^{-2}	7.0×10^{-3}
3	14.195	2	4.5×10^{-3}	2.17	1.385×10^{-2}	9.0×10^{-3}
4	24.54	3	1.8×10^{-3}	1.67	4.17×10^{-3}	3.6×10^{-3}
5	24.54	3	3.5×10^{-3}	2.49	1.199×10^{-2}	7.0×10^{-3}
6	24.54	4	4.5×10^{-3}	2.587	1.639×10^{-2}	9.0×10^{-3}

Table 2
Local bulk properties for LES

LES cases	Re_b	T_w/T_b	Gr_q/Re_b^2	Nu_b	K_v	B_j
1	5728.28	1.40	0.116	15.55	9.9×10^{-7}	3.519×10^{-7}
2	5130.51	1.91	0.15	11.04	2.03×10^{-6}	5.36×10^{-7}
3	3683.37	2.02	0.202	8.86	4.6×10^{-6}	1.188×10^{-6}
4	5401.89	1.44	0.04	13.70	1.097×10^{-6}	1.325×10^{-7}
5	4820.86	1.84	0.073	9.49	2.12×10^{-6}	2.868×10^{-7}
6	3270.6	2.09	0.246	7.32	4.8×10^{-6}	1.73×10^{-6}

Table 3
Local bulk properties for corresponding experiments

LES cases	Experiments	Re_b	T_w/T_b	Gr_q/Re_b^2	Nu_b	K_v	B_j
1	Run 618 ($x/D = 14.195$)	5653	1.42	0.11	15.57	1.2×10^{-6}	3.404×10^{-7}
2	Run 635 ($x/D = 19.87$)	5037	1.88	0.13	11.40	2.2×10^{-6}	4.781×10^{-7}
3	Run 445 ($x/D = 14.195$)	3595	1.96	0.3	9.5	4×10^{-6}	1.83×10^{-6}
4	Run 618 ($x/D = 24.54$)	5408	1.43	0.09	13.6	1.15×10^{-6}	2.976×10^{-7}
5	Run 635 ($x/D = 24.54$)	4894	1.89	0.12	10.21	2.1×10^{-6}	4.61×10^{-7}
6	Run 445 ($x/D = 24.54$)	3280	1.97	0.19	7.45	3.56×10^{-6}	1.33×10^{-6}

$$B_j = \frac{Gr}{Re_b^{3.425} Pr^{0.8}}. \tag{29}$$

Kline et al. [22] found that turbulent bursts appeared to cease when K_v reached a critical value of about 3.7×10^{-6}, and Chambers et al. [23] indicated that the bursting rate remained approximately constant at the turbulent value when K_v was about 1.5×10^{-6} or less. Therefore, by these criteria, the current simulations were expected to be located in a range from fully turbulent to "laminarizing". Jackson estimated that the effect of buoyancy on the heat transfer of developed turbulent pipe flow could be negligible when B_j is less than about 5.6×10^{-7} [24]. According to this criterion and the values of B_j in Table 2, forced convection should dominate in the current simulations.

To validate the present results further, the mean streamwise velocity and temperature distributions were compared with the experimental results obtained by Shehata and McEligot [5]. Profiles of the mean streamwise velocity in wall coordinates (indicated by the '+' superscripts for y and u) where

$$u^+ = \frac{u}{u_\tau}, \quad u_\tau = \sqrt{\frac{\tau_w}{\rho_w}}, \quad y^+ = \frac{(R-r)u_\tau}{\nu_w} \tag{30}$$

are plotted in Fig. 2 for cases 1–6. The results agree well with the experimental profiles. The mean temperature difference is given in wall coordinates as

$$\theta^+ = \frac{T - T_w}{T_\tau}, \quad T_\tau = \frac{q''_w}{\rho_w c_p u_\tau} \tag{31}$$

and the distributions of θ^+ for cases 1–6 are shown in Fig. 3. The figures show good agreement between experimental results and the LES simulations. The trend toward laminarization can be observed in Fig. 4 where the temperature profiles for all six cases are compared with a laminar temperature profile evaluated at the conditions of Run 445 [5]. The temperature profile for the highest heating case, 6, is seen to fall close to the

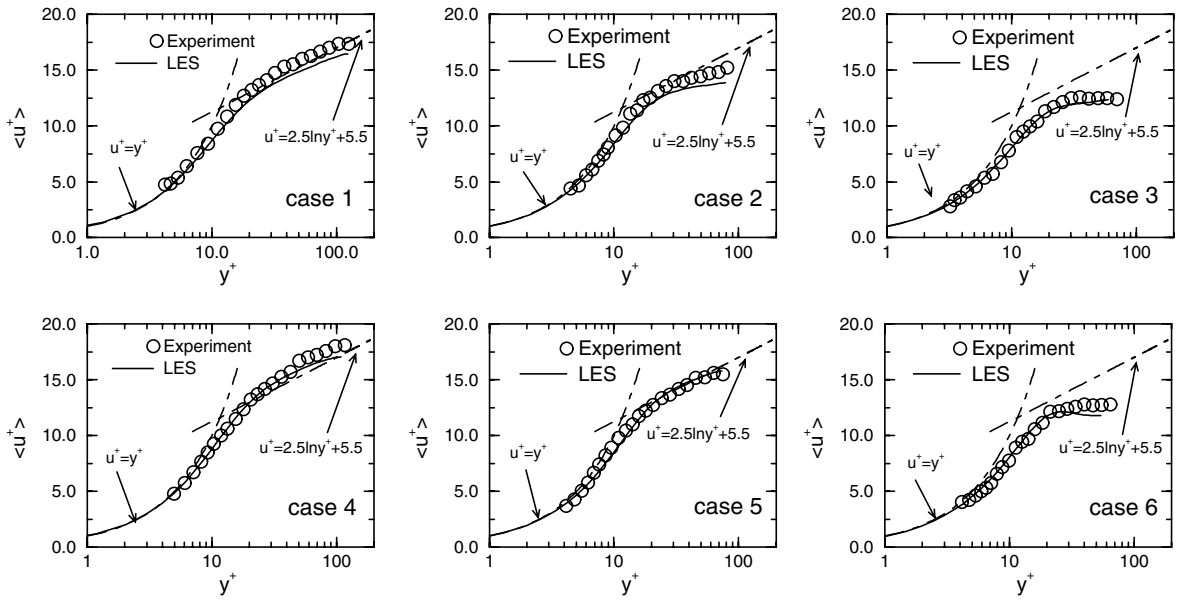

Fig. 2. Comparison of simulated and experimental streamwise mean velocity profiles.

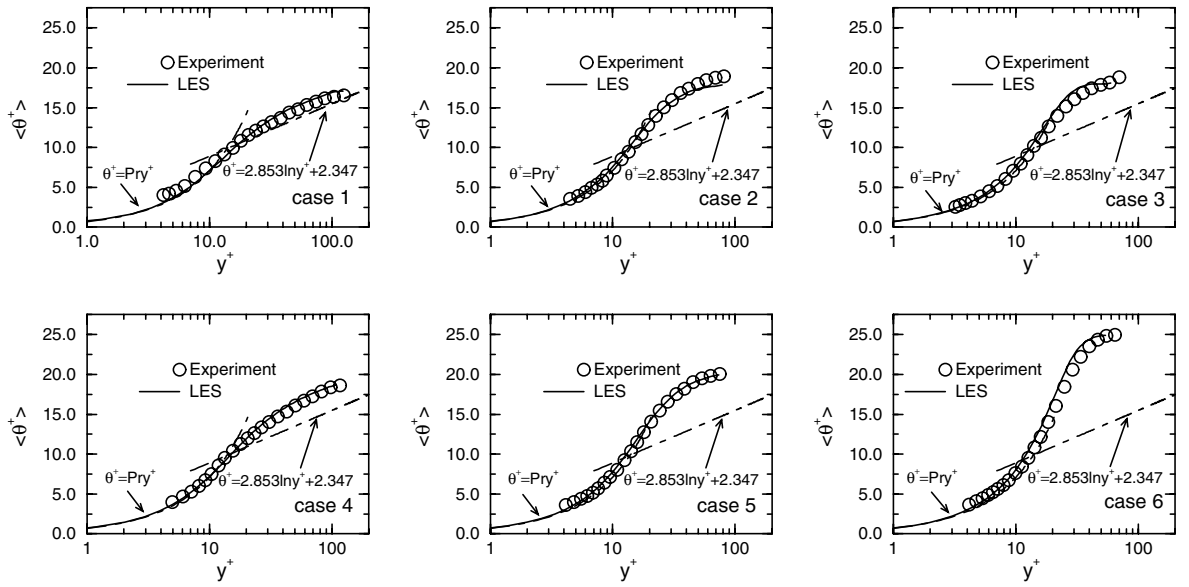

Fig. 3. Comparison of simulated and experimental mean temperature profiles.

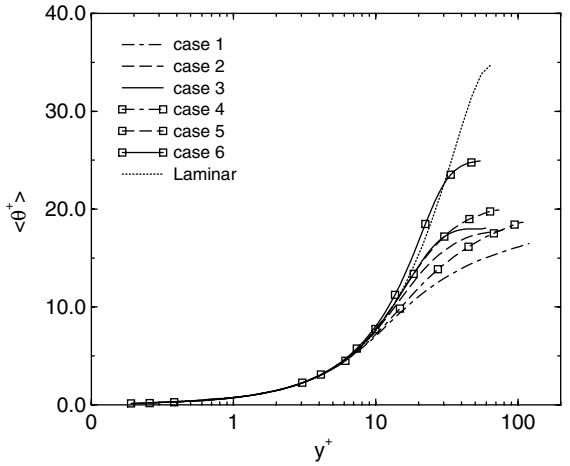

Fig. 4. Predicted mean temperature profiles in wall coordinates.

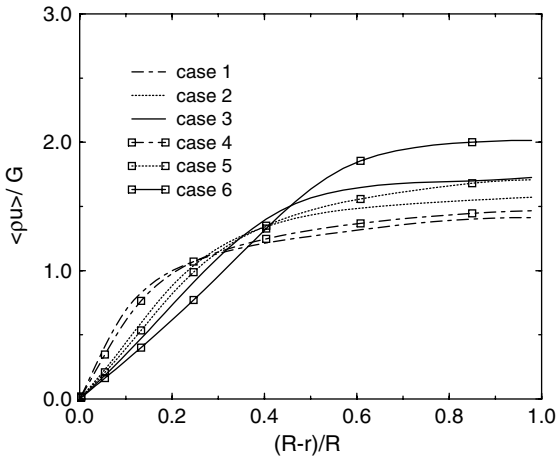

Fig. 5. Predicted mean streamwise momentum profiles normalized by mean mass flux.

laminar profile and the semi-logarithmic region has nearly vanished.

The distributions of mean streamwise momentum, $\langle \rho u \rangle$, normalized by mean mass flux, G, in cases 1–6 are plotted in Fig. 5, which shows that the profile was fairly flat when the heating rate was small. However, the profile became much more parabolic when the nondimensional heating rate was $q_{\text{in}} = 0.0045$. The mass flow was redistributed toward the center of the pipe due to the high heating.

The velocity fluctuations in the streamwise, radial, and circumferential directions normalized by friction velocity for cases 1–6 are plotted against y^+ in Fig. 6. A comparison of these indicates that the turbulent intensities decreased as the nondimensional heating rate increased. Such a decrease is consistent with the effectively thickened viscous layers. Chambers [23] also observed that the acceleration of a turbulent flow reduces the apparent turbulent bursting rate near the wall, which will lead to the suppression of velocity fluctuations. Consequently, the larger acceleration parameter, K_v, results in lower turbulence intensities. The same trend was found in this research.

Fig. 7 shows the resolved, viscous, and SGS shear stress profiles normalized by the wall shear stress. The shear stresses are defined as

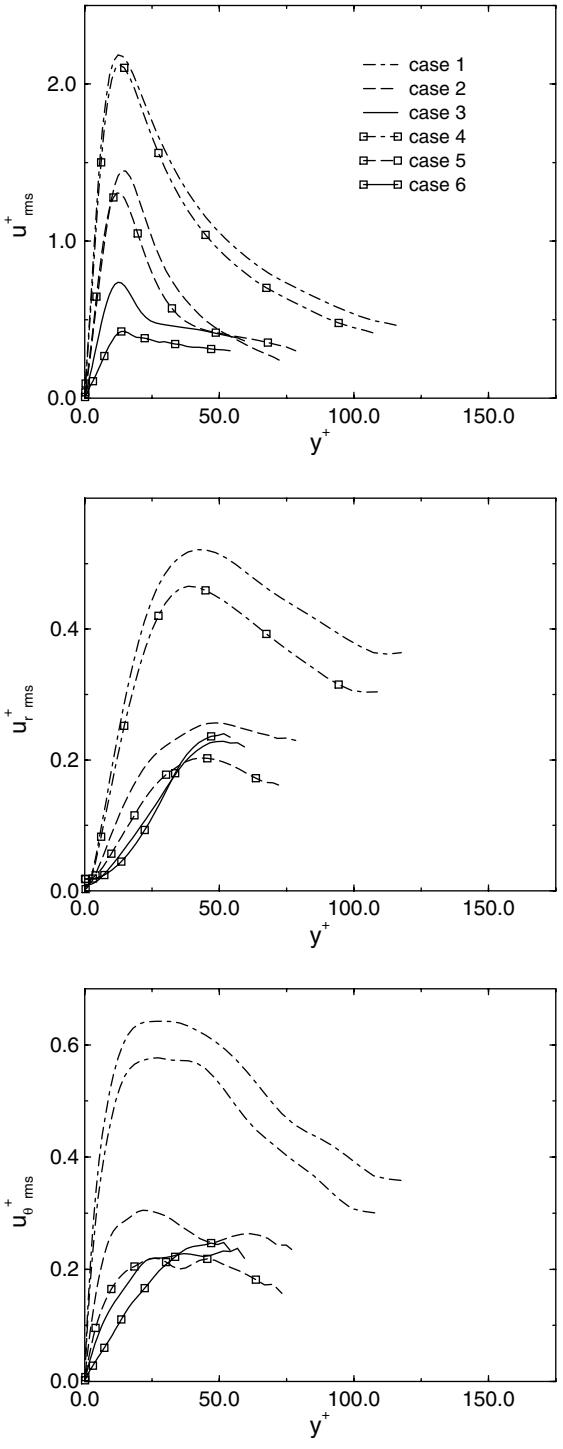

Fig. 6. Predicted velocity fluctuations in wall coordinates.

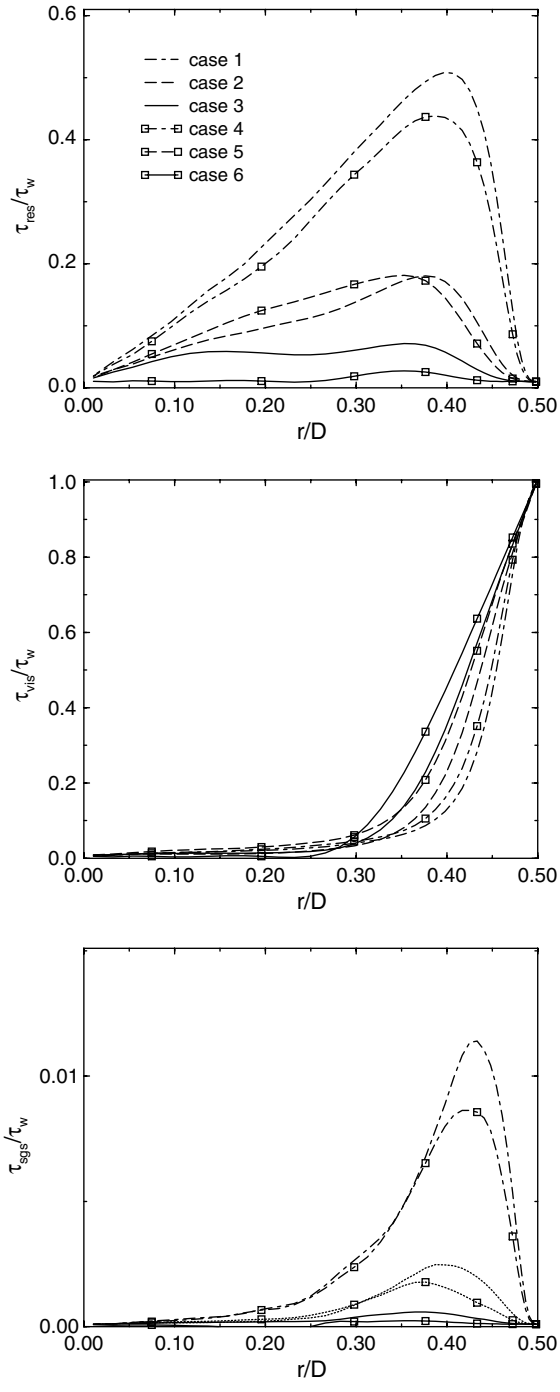

Fig. 7. Predicted shear stress distributions normalized by wall shear stress.

$$\tau_{\mathrm{res}} = -\langle \rho u'' u_{\mathrm{r}}'' \rangle, \tag{32}$$

$$\tau_{\mathrm{vis}} = -\left\langle \mu \frac{\partial u}{\partial r} \right\rangle, \tag{33}$$

$$\tau_{\mathrm{sgs}} = -\left\langle \mu_{\mathrm{t}} \frac{\partial u}{\partial r} \right\rangle, \tag{34}$$

where $''$ denotes the Favre average. As shown in the figure, shear stresses decreased when the heat fluxes in-

creased. The turbulent structures may not be maintained in cases 3 and 6 due to the small resolved shear stresses, and the flow may not have much turbulent momentum transport. The resolved heat flux, heat conduction, and modeled SGS heat flux distributions normalized by the wall heat flux are shown in Fig. 8, where

$$q_{\mathrm{res}} = -\langle \rho u_{\mathrm{r}}'' T'' \rangle, \tag{35}$$

$$q_{\mathrm{con}} = -\left\langle \frac{\mu c_p}{Pr} \frac{\partial T}{\partial r} \right\rangle, \tag{36}$$

$$q_{\mathrm{sgs}} = -\left\langle \frac{\mu_{\mathrm{t}} c_p}{Pr_{\mathrm{t}}} \frac{\partial T}{\partial r} \right\rangle. \tag{37}$$

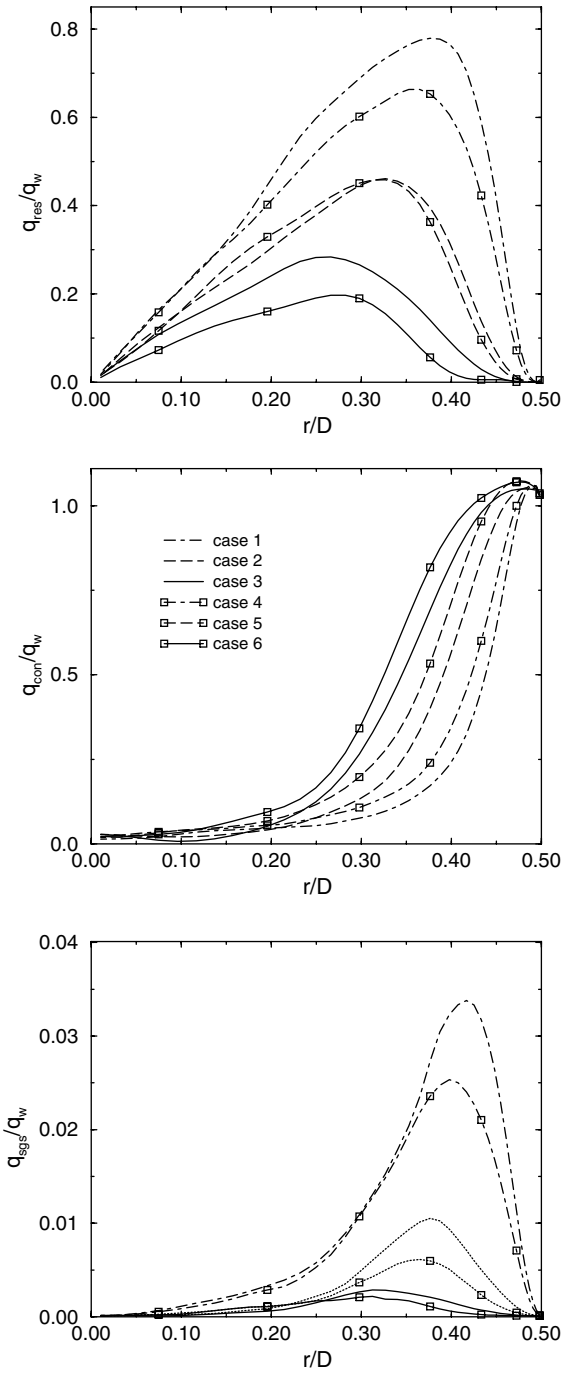

Fig. 8. Predicted heat flux distributions normalized by wall heat flux.

The same trends were observed as for shear stresses. The significantly reduced turbulent heat fluxes in cases 3 and 6 are due to the effectively thickened viscous layer which is believed to be responsible for the main thermal resistance in the flow.

The instantaneous velocity vector plots in the middle plane of the pipe for cases 1–6 are shown in Fig. 9. The large scale motions that account for most of energy are clearly shown near the wall region in cases 1 and 4. Head and Bandyopadhyay [25] suggested that larger-scale structures can be composed of an ensemble of hairpin vortices, which maintain the turbulence in the flow. The decaying of hairpin vortices can be observed in cases 2 and 5, where the large eddies moved toward center of the pipe and the eddies are smaller and not obvious compared to those in cases 1 and 4. The vector plots for cases 3 and 6 are similar to that of laminar pipe flow; almost no large scale motion was observed, which may be evidence of "laminarization".

6. Conclusions

Large eddy simulations of vertical turbulent pipe flows with high heat transfer have been accomplished for the downstream conditions of the experiments by Shehata and McEligot [5] using a quasi-developed approach. The results have been validated by comparing the integral parameters and mean streamwise velocity and temperature profiles to the experimental data. It is observed that the integral parameters agreed well with experimental data and the values of the buoyancy parameter indicated that forced convection dominated in the simulations. The Nusselt number decreased when the heat rate increased possibly due to thicker viscous layer. Very good agreement of the mean streamwise velocity and temperature profiles with experiments has been obtained. It is shown that the mass flow was redistributed toward the center of the pipe due to the high heating and the profile became more parabolic-like at higher heat transfer rates. The plots of velocity fluctuations indicated that high heating rates suppressed the turbulent intensities due to the significantly thickened viscous layer. The high heating rates resulted in significant property variations leading to a remarkable reduction of Reynolds shear stresses and heat fluxes.

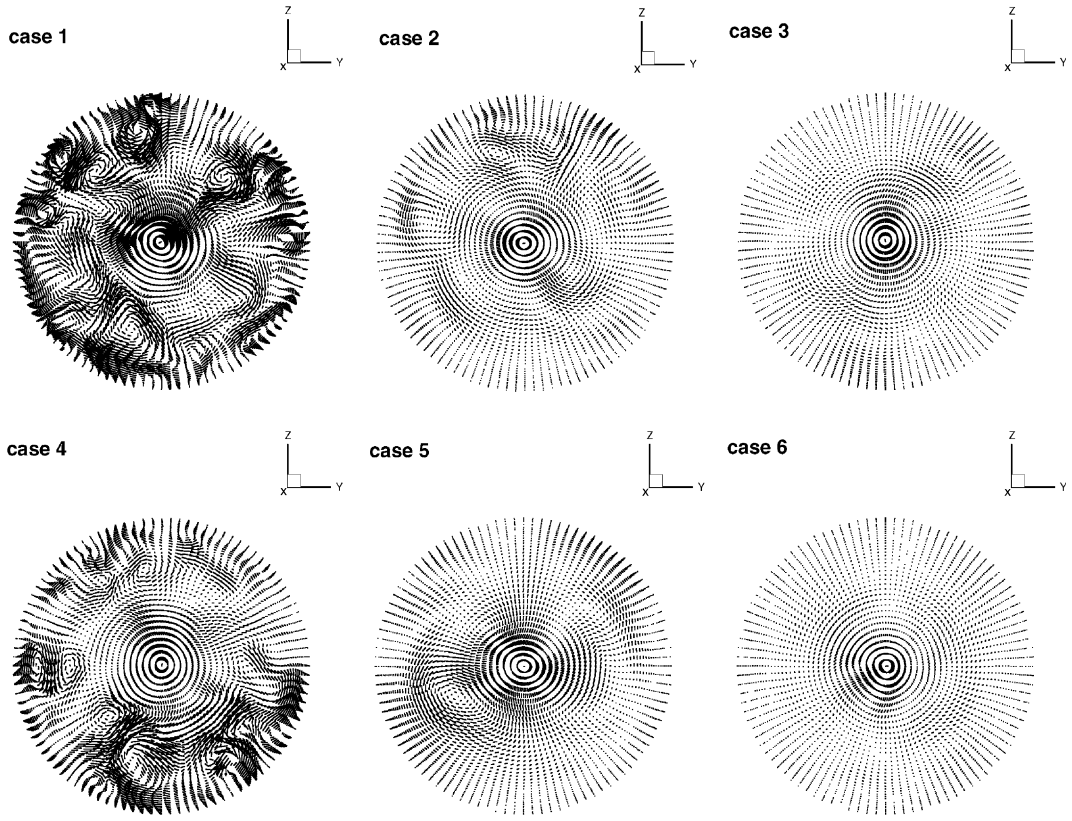

Fig. 9. Predicted instantaneous velocity vector plots in the middle plane of pipe.

Large scale motions were clearly evident near the wall region for the turbulent cases, cases 1 and 4, but no large eddies were visible near the wall for the "laminarizing" cases, cases 3 and 6.

Acknowledgements

The authors are grateful to the Department of Energy for support through grant DE-FG03-995F21924 under the NERI program and through DOE/NE Idaho Operations Office contract DE-AC07-99ID13727 under the I-NERI program. Iowa State High Performance Computing Center and University of Minnesota Supercomputing Institute provided computational resources needed for this research.

References

[1] D.M. McEligot, Convective heat transfer in internal gas flows with temperature-dependent properties, Adv. Transp. Pr. 4 (1986) 113–200.
[2] S. Torii, W.-J. Yang, Laminarization of turbulent gas flow inside a strongly heated tube, Int. J. Heat Mass Transfer 40 (1997) 3105–3117.
[3] K. Ezato, A.M. Shehata, T. Kunugi, D.M. McEligot, Numerical prediction of transitional features of turbulent forced gas flows in circular tubes with strong heating, J. Heat Transfer 121 (1999) 546–555.
[4] K.R. Perkins, Turbulence structure in gas flows laminarizing by heating, Ph.D. thesis, University of Arizona, 1975.
[5] A.M. Shehata, D.M. McEligot, Mean structure in the viscous layer of strongly-heated internal gas flows. Measurements, Int. J. Heat Mass Transfer 41 (1998) 4297–4313.
[6] D.P. Mikielewicz, Comparative studies of turbulent models under conditions of mixed convection with variable properties in heated vertical tubes, Ph.D. thesis, University of Manchester, 1994.
[7] J. Kim, P. Moin, R. Moser, Turbulence statistics in fully developed channel flow at low Reynolds number, J. Fluid Mech. 177 (1989) 133–166.
[8] W.-P. Wang, R.H. Pletcher, On the large eddy simulation of a turbulent channel flow with significant heat transfer, Phys. Fluids 8 (1996) 3354–3366.
[9] O. Iida, N. Kasagi, Direct numerical simulation of unsteady stratified turbulent channel flow, J. Heat Transfer 119 (1997) 53–61.
[10] L.D. Dailey, R.H. Pletcher, Large eddy simulation of constant heat flux turbulent channel flow with property variations, AIAA paper 98-0791.
[11] F. Nicoud, T. Poinsot, DNS of a channel flow with variable properties, in: Proceedings of the First Interna-

tional Symposium of Turbulence and Shear Flow Phenomena, Santa Barbara, California, 1999, pp. 697–702.
[12] S. Satake, T. Kunugi, A.M. Shehata, D.M. McEligot, Direct numerical simulation for laminarization of turbulent forced gas flows in circular tubes with strong heating, Int. J. Heat Fluid Flow 21 (2000) 526–534.
[13] D.M. McEligot, S.B. Smith, C.A. Bankston, Quasi-developed turbulent pipe flow with heat transfer, J. Heat Transfer 92 (1970) 641–650.
[14] A.W. Vreman, B.J. Geurts, H. Kuerten, Subgrid-modeling in LES of compressible flow, Appl. Sci. Res. 54 (1995) 191–203.
[15] T. Cebeci, A.M.O. Smith, Analysis of Turbulent Boundary Layers, Academic Press, New York, 1974.
[16] P. Moin, K. Squires, W. Cabot, S. Lee, A dynamic subgrid-scale model for compressible turbulence and scalar transport, Phys. Fluids A 3 (1991) 2746–2757.
[17] D.K. Lilly, A proposed modification of the Germano subgrid-scale closure method, Phy. Fluids A 4 (1992) 633–635.
[18] X.-F. Xu, Large eddy simulation of compressible turbulent pipe flow with heat transfer, Ph.D. thesis, Iowa State University, 2003.
[19] X.-F. Xu, J.S. Lee, R.H. Pletcher, Cartesian based finite volume formulation for LES of mixed convection in a vertical turbulent pipe flow, in: Proceedings of ASME International Mechanical Engineering Congress Exposition, New Orleans, LA, 2002, paper IMECE2002-HT-32748.
[20] J.G.M. Eggels, F. Unger, M.H. Weiss, J. Westerweel, R.J. Adrian, R. Friedrich, F.T.M. Nieuwstadt, Fully developed turbulent pipe flow: a comparison between direct numerical simulation and experiment, J. Fluid Mech. 268 (1994) 175–209.
[21] J. Westerweel, J.G.T.H. Draad, van der Hoeven, J. van Oord, Measurement of fully-developed turbulent pipe flow with digital particle image velocimetry, Exp. Fluids 20 (1996) 165–177.
[22] S.J. Kline, W.C. Reynolds, F.A. Schraub, P.W. Rundstadler, The structure of turbulent boundary layers, J. Fluid Mech. 30 (1967) 741–773.
[23] F.W. Chambers, H.D. Murphy, D.M. McEligot, Laterally converging flow. Part 2. Temporal wall shear stress, J. Fluid Mech. 127 (1983) 403–428.
[24] D.P. Mikielewicz, A.M. Shehata, J.D. Jackson, D.M. McEligot, Temperature, velocity and mean turbulence structure in strongly heated internal gas flows comparison of numerical predictions with data, Int. J. Heat Mass Transfer 45 (2002) 4333–4352.
[25] R.M. Head, P. Bandyopadhyay, New aspects of turbulent boundary layer structure, J. Fluid Mech. 107 (1981) 238–297.